arXiv:1109.1188v1 [hep-ex] 6 Sep 2011

Partial Wave Analysis of $\bar{p}p \to \pi^-\pi^+$, $\pi^0\pi^0$, $\eta\eta$ and $\eta\eta'$

A.V. Anisovich[c], C.A. Baker[a], C.J. Batty[a], D.V. Bugg[b], A. Hasan[b], C. Hodd[b], J. Kisiel[d], V.A. Nikonov[c], A.V. Sarantsev[c], V.V. Sarantsev[c], B.S. Zou[b] [1]

[a] *Rutherford Appleton Laboratory, Chilton, Didcot OX11 0QX,UK*

[b] *Queen Mary and Westfield College, London E1 4NS, UK*

[c] *PNPI, Gatchina, St. Petersburg district, 188350, Russia*

[d] *University of Silesia, Katowice, Poland*

Abstract

A partial wave analysis is presented of Crystal Barrel data on $\bar{p}p \to \pi^0\pi^0$, $\eta\eta$ and $\eta\eta'$ from 600 to 1940 MeV/c, combined with earlier data on $d\sigma/d\Omega$ and P for $\bar{p}p \to \pi^-\pi^+$. The following s-channel $I = 0$ resonances are identified: (i) $J^{PC} = 5^{--}$ with mass and width (M, Γ) at (2295 ± 30, 235^{+65}_{-40}) MeV, (ii) $J^{PC} = 4^{++}$ at (2020 ± 12, 170 ± 15) MeV and (2300 ± 25, 270 ± 50) MeV, (iii) $^3D_3$ $J^{PC} = 3^{--}$ at (1960 ± 15, 150 ± 25) MeV and (2210 ± 40, 360 ± 55) MeV, and a $^3G_3$ state at ($2300^{+50}_{-80}, 340 \pm 150$) MeV, (iv) $J^{PC} = 2^{++}$ at (1910 ± 30, 260 ± 40) MeV, (2020 ± 30, 275 ± 35) MeV, (2230 ± 30, 245 ± 45) MeV, and (2300 ± 35, 290 ± 50) MeV, (v) $J^{PC} = 1^{--}$ at (2005 ± 40, 275 ± 75) MeV, and (2165 ± 40, 160^{+140}_{-70}) MeV, and (vi) $J^{PC} = 0^{++}$ at (2005 ± 30, 305 ± 50) MeV, (2105 ± 15, 200 ± 25) MeV, and (2320 ± 30, 175 ± 45) MeV. In addition, there is a less well defined 6^{++} resonance at 2485 ± 40 MeV, with $\Gamma = 410 \pm 90$ MeV. For every J^P, almost all these resonances lie on well defined linear trajectories of mass squared v. excitation number. The slope is 1.10 ± 0.03 Gev^2 per excitation.

The $f_0(2105)$ has strong coupling to $\eta\eta$, but much weaker coupling to $\pi^0\pi^0$. Its flavour mixing angle between $q\bar{q}$ and $s\bar{s}$ is $(59 - 71.6)^\circ$, i.e. dominant decays to $s\bar{s}$. Such decays and its strong production in $\bar{p}p$ interactions strongly suggest exotic character.

PACS: 13.75Cs, 14.20GK, 14.40
Keywords: mesons, resonances, annihilation

1 Introduction

In an accompanying paper [1], data are presented from the Crystal Barrel experiment on $\bar{p}p \to \pi^0\pi^0$, $\eta\eta$ and $\eta\eta'$ at nine beam momenta from 600 to 1940 MeV/c; this corresponds to the mass range 1960–2410 MeV. The objective of the present paper is to add these new results to earlier data on $\bar{p}p \to \pi^-\pi^+$ and do a combined partial wave analysis. Data on $d\sigma/d\Omega$ were reported by Eisenhandler et al. [2] and on polarisation P by Carter et al. [3] from 990 to 2430 MeV/c (masses up to 2580 MeV). Further data on both $d\sigma/d\Omega$ and P from 360 to 1550 MeV/c were reported by Hasan et al. [4]. The polarisation data play a vital role in the analysis, since they separate cleanly states with $L = J \pm 1$, e.g. $^3P_2$ and $^3F_2$. These data help greatly in consolidating the analyses of $\pi^0\pi^0$, $\eta\eta$ and $\eta\eta'$ data and help identify resonances. The data of Hasan et al. are particularly valuable, since they cover the important mass range down to 1910 MeV.

[1] Now at IHEP, Beijinj 100039, China

There have been several earlier amplitude analyses of the data on $\bar{p}p \to \pi^-\pi^+$ [5-11]. We find quite good agreement with these papers, though we locate additional features, noteably four 2^+ states. The earlier analyses were restricted to the $\pi\pi$ channel only. One of our primary objectives is to include $\eta\eta$ and $\eta\eta'$ data, so as to examine the SU(3) character of the fitted resonances.

We also use data on 4^+ states observed in $\bar{p}p \to \eta\pi^0\pi^0$ [12]. They provide further constraints on the relative sign and magnitudes of ${}^3H_4$ and ${}^3F_4$ amplitudes.

The analysis reported here is in terms of s-channel resonances up to $J^{PC} = 6^{++}$, plus backgrounds which are needed only in the low partial waves 0^{++} and 1^{--}. There are a number of reasons for this approach in terms of resonances. Firstly, we find that the well known $f_4(2050)$ makes a large and unavoidable contribution. It fits to a mass and width slightly lower than averages quoted by the Particle Data Group (PDG) [13]. Because we need to make use of its fitted mass, we shall hereafter refer to it as $f_4(2020)$. Once this resonance is introduced, it defines phases over a considerable mass range. Relative phases with other partial waves are accurately determined and it becomes impossible to avoid introducing further resonances into all other partial waves. This is not surprising, since resonances are predicted in this mass range by extrapolation from experience at lower masses. A second related point concerns the polarisation. It lies close to +1 over much of the angular range at many momenta and inevitably requires large imaginary parts in many partial wave amplitudes. The quantity $Pd\sigma/d\Omega$ is proportional to the imaginary part of the interference between partial waves. Differential cross sections measure the real parts of the same interferences. In order to achieve consistency between the principle of analyticity and these real and imaginary parts of interferences, we find resonance behaviour in all partial waves unavoidable. This is what was found in all earlier analyses except that of Kloet and Myrher [11], which focussed on the narrow mass range below a momentum of 1 GeV/c.

2 Procedures and Formulae

For completeness, we repeat the standard formulae used in earlier work. The differential cross section may be expressed in terms of spin-flip (F_{+-}) and non-flip (F_{++}) helicity amplitudes:

$$d\sigma/d\Omega = |F_{++}|^2 + |F_{+-}|^2 \quad (1)$$

$$F_{++} = \frac{1}{4}\sum_{J=0}^{J_{max}} (2J+1) f^J_{++} P_J(\cos\theta) \quad (2)$$

$$F_{+-} = \frac{1}{4}\sum_{J=1}^{J_{max}} \frac{(2J+1)}{\sqrt{J(J+1)}} f^J_{+-} P^1_J(\cos\theta). \quad (3)$$

Here P^m_J are Legendre polynomials. Partial helicity amplitude f^J are defined in terms of angular momentum partial waves $T_{L,J}$ according to:

$$\sqrt{2J+1} f^J_{++} = \sqrt{J} T_{J-1,J} - \sqrt{J+1} T_{J+1,J} \quad (4)$$

$$\sqrt{2J+1} f^J_{+-} = \sqrt{J+1} T_{J-1,J} + \sqrt{J} T_{J+1,J}. \quad (5)$$

Our procedure is to express the $T_{L,J}$ as sums over resonances, up to 5 for each J value:

$$T_{L,J} = \sum_{i=1}^{5} \frac{G_i B_L(p) B_J(q) \exp(i\phi_i)}{M_i^2 - s - iM_i\Gamma_i}. \tag{6}$$

Here B_L are standard Blatt-Weisskopf centrifugal barrier factors for angular momentum L in terms of momentum p in the entrance channel $\bar{p}p$ and q in the exit meson channel. Explicit formulae are given by Chung [14]. They guarantee the correct threshold behaviour in the $\bar{p}p$ channel. The G_i are real coupling constants and ϕ_i are phases for each resonance, arising from final state interactions.

We now comment in general terms on this approach. Firstly, resonances overlap and interact to some degree, e.g. via common decay channels. In principle, a K-matrix approach is desirable, in order to investigate such interactions. In reality, this is impracticable at present, because of the large number of open channels, and almost complete lack of information about many of them. A practical point is that the speed of convergence of the fitting procedure is helped greatly by using as basis states the eigenstates of the scattering amplitudes; these are T-matrix poles. We therefore view the resonances fitted to the data as a parametrisation from which further analysis can unfold the physics content. A first step is to find how many resonances are required and what their properties are.

A second concern is that t-channel exchanges also undoubtedly contribute. What effect are they likely to have, if any? In each partial wave, they lead to left-hand singularities which are very distant; the left-hand cut opens below $s \simeq 1$ GeV^2. For $J \leq 3$, there are further resonances lying between the mass range discussed here and the left-hand cuts. Any t-channel amplitude will acquire the phase dictated by s-channel resonances in each partial wave, via rescattering within the present mass range. The effect of any t-channel exchange is therefore to introduce some slow s-dependence into the resonance width. A classic example of this is the effect of the nucleon pole on the shape of the $\Delta(1232)$ resonance, first treated by the theory of Chew and Low [15]. In the present mass range, fitting an s-dependent width to each resonance is an impractical luxury, because there are too many unknowns. For example, form factors and the opening of new channels will distort the shape of each resonance. For simplicity, we adopt constant widths.

One of our objectives is to examine the SU(3) content of resonances. The simplest approach would be to require each resonance to have the same phase ϕ_i for all its decay channels. Secondly, amplitudes for decay to $\eta\eta$ and $\eta\eta'$ are in principle related to those for $\pi\pi$ via the quark content of the resonance, and via the well-known composition of η and η' in terms of singlet and octet states and the pseudoscalar mixing angle Θ :

$$|q\bar{q}> \;=\; \cos\Theta|\eta> + \sin\Theta|\eta'> \tag{7}$$

$$|s\bar{s}> \;=\; -\sin\Theta|\eta> + \cos\Theta|\eta'>, \tag{8}$$

where $\cos\Theta \simeq 0.8$ and $\sin\Theta \simeq 0.6$ [13]. Amplitudes for decay of $I = 0$ $q\bar{q}$ combinations to $\pi^0\pi^0$, $\eta\eta$ and $\eta\eta'$ may then be written compactly as:

$$f(q\bar{q}) \;=\; \frac{|\pi^0\pi^0>}{\sqrt{2}} + \frac{\cos^2\Theta}{\sqrt{2}}|\eta\eta> + \cos\Theta\sin\Theta|\eta\eta'>, \tag{9}$$

$$f(s\bar{s}) \;=\; \sqrt{\lambda}[\sin^2\Theta|\eta\eta> + \cos^2\Theta|\eta\eta'> - \sqrt{2}\cos\Theta\sin\Theta|\eta\eta'>]. \tag{10}$$

We have introduced into the latter equation a factor λ. This factor has been fitted empirically in Ref. [16] to a large variety of data on strange and non-strange final states at high energies. Its value is $\sqrt{\lambda} = 0.8 - 0.9$ and we adopt the central value of 0.85.

The resonances R we observe in present data may be linear combinations of $q\bar{q}$ and $s\bar{s}$:

$$R = \cos\Phi|q\bar{q}> + \sin\Phi|s\bar{s}> . \tag{11}$$

We use $q\bar{q}$ as a shorthand to denote $(u\bar{u} + d\bar{d})/\sqrt{2}$. We expect the observed resonances to be dominantly $q\bar{q}$ in view of their production in $\bar{p}p$ reactions; however, we would like to test this against the observed branching ratios to $\pi\pi$, $\eta\eta$ and $\eta\eta'$. Amplitudes for the decay of R to these three channels are given by the three equations:

$$f(\pi^0\pi^0) = \frac{\cos\Phi}{\sqrt{2}} \tag{12}$$

$$f(\eta\eta) = \frac{\cos\Phi}{\sqrt{2}}(\cos^2\Theta + \sqrt{2\lambda}\sin^2\Theta\tan\Phi) \tag{13}$$

$$f(\eta\eta') = \frac{\cos\Phi}{\sqrt{2}}\cos\Theta\sin\Theta(1 - \sqrt{2\lambda}\tan\Phi). \tag{14}$$

In our earliest attempts to fit data on $\eta\eta$ and $\eta\eta'$, it immediately became obvious that there are major problems in applying these SU(3) relations. The best fit we shall show later has a χ^2 of 10585. If one sets the phase angles ϕ_i of each resonance to the same value in all three decay channels $\pi^0\pi^0$, $\eta\eta$ and $\eta\eta'$ and takes the resonances to be pure $q\bar{q}$, χ^2 increases dramatically to about 45000. The fit is visibly awful. Some deviation from strict $SU(3)$ is obviously required. It is necessary to introduce some latitude into phase angles ϕ_i to different channels, or into the flavour composition of the resonances, or both.

To examine where the problem lies, we have tried fitting two extreme scenarios. The first is to take all resonances to be pure $q\bar{q}$ by setting all Φ to zero; if the phases ϕ_i of all resonances are left free, $\chi^2 \to 14558$. This is not a huge increase in χ^2 over our best value of 10585. However, the fit to both $\eta\eta$ and $\pi^0\pi^0$ angular distributions is visibly poor, particularly for $\eta\eta$. Furthermore, some of the phases ϕ_i depart from zero by unreasonably large amounts $> 90°$. So it seems that some departure from strict SU(3) is unavoidable.

The other extreme is to set all ϕ_i to zero and attempt to fit purely by adjusting flavour mixing angles Φ. This turns out to be more successful, giving a χ^2 of 11527. We shall give detailed results below. Most of the mixing angles optimise in the range 0–20°, i.e. close to pure $q\bar{q}$ states. These small mixing angles allow modest changes in branching ratios between $\pi^0\pi^0$, $\eta\eta$ and $\eta\eta'$. However, one resonance, $f_0(2105)$, requires considerably larger mixing, with Φ in the range 59–71.6°. The integrated cross sections shown below for $\pi^0\pi^0$, $\eta\eta$ and $\eta\eta'$ are fairly close to the values predicted by simple SU(3) on average. The question therefore is whether it is wise to set phase angles ϕ_i strictly at zero. We now consider several considerations bearing on this point.

Firstly, each resonance rides on the tails of other resonances. We have had experience of fitting data at lower masses by both T-matrix techniques [17] and the K-matrix [18]. From this experience, we have learned that mixing between states commonly gives rise to deviations of phase angles ϕ_i betweeen different decay channels in the range –15 to +15°. Even if K-matrix poles have the same phases, T-matrix poles can have different phases; the difference depends

on the separation of poles, resonances widths and the mixing through decay channels. In view of this experience, we feel it unwise to demand strictly the same phases ϕ_i in all channels. For most resonances, we have allowed ϕ_i to optimise freely for each decay channel with differences limited to the range –15 to +15°. In isolated cases, where they seem to need it, this range has been allowed to extend to ±30°.

Angles Φ for flavor mixing mostly optimise naturally in the range –15 to +15 °. However, for large spin, it is likely that differences in centrifugal barriers and form factors between $\pi\pi$, $\eta\eta$ and $\eta\eta'$ may affect branching ratios. Resonances are commonly believed to have radii of 0.8–1.0 fm. In $\pi\pi$ decays, the wavelength of each outgoing π is 1.1 fm for a resonance mass of 2.2 GeV. Overlap of wave functions will play a strong role in determining matrix elements. Even quite small momentum differences between $\pi\pi$ and $\eta\eta$ and larger differences for $\eta\eta'$ may lead to significant departures from SU(3). We observe a problem in fitting $\eta\eta$ cross sections simultaneously with $\pi^0\pi^0$ unless some departure from strict SU(3) is allowed. Our final compromise is therefore to allow flavour mixing angles to vary in the range 0 to ±30°. All optimise naturally in this range, except for $f_0(2105)$, which must be allowed complete freedom. As far as resonance masses and widths are concerned, the freedom in flavour mixing angles fortunately has little effect; masses and widths are determined by the locations of singularities, which are independent of mixing and corresponding branching ratios.

A further unknown is the radius to be given to centrifugal barriers. The masses fitted to 4^+ states are sensitive to this radius, since the centrifugal barrier in the $\bar{p}p$ channel is strong. If the $f_4(2020)$ is to be fitted to the PDG value of 2044 MeV, the radius required is unreasonably large, namely 1.5 fm. The fitted value is 0.88 fm.

Ratios of amplitudes for $L = J \pm 1$, i.e. $r_J = |f_{J+1}|/|f_{J-1}|$ are fitted to real constants for each resonance. Since this linear combination refers to mixing within the $\bar{p}p$ channel, it is taken to be the same for decays to $\pi\pi$, $\eta\eta$ and $\eta\eta'$. For the $f_4(2020)$, one expects the channel with $L = J-1$ to dominate over $L = J+1$, because of the centrifugal barrier. This is precisely what we find. Likewise, the 5^- state is dominantly ${}^3G_5$. This mixing is determined very precisely by the polarisation data. For 6^+, we assume pure ${}^3H_6$.

The data on $\pi^0\pi^0$, $\eta\eta$ and $\eta\eta'$ stop at 1940 MeV/c. Polarisation data stop at 2200 MeV/c. From $\pi^-\pi^+$ data above 2 GeV/c, it is clear that a 6^+ resonance is required at 2485 ± 40 MeV. A resonance close to this mass has been observed decaying to $\pi\pi$ by the GAMS collaboration [19], at 2510 MeV. It seems likely that there will be further high spin resonances of similar mass. They lie so close to the top of the available mass range that we cannot establish their parameters precisely. Nonetheless, it is convenient to use 5^-, 4^+, and 2^+ resonances in the range 2500–2620 MeV to parametrise the data at the highest momenta. The tail of the 6^+ resonance in the mass range LEAR below 2410 MeV needs to be described accurately, since its interferences with states of lower spin are important for fitting Legendre polynomials up to order 10 required by the $\pi\pi$ and $\eta\eta$ data.

3 Results

We summarise first the expected states. The $f_4(2020)$ is well known and there is plenty of evidence, summarised by the Particle Data Group, for its radial excitation $f_4(2300)$. There is a known ρ_5 at 2330 MeV. Consequently, resonances having spins with all J^P below 4^+ are

expected around 2020 MeV and with all J^P below 5^- around 2300 MeV. In the mass range 1910–2410 MeV, our main focus of attention, this implies two ${}^3D_3$ $q\bar{q}$ states plus one with ${}^3G_3$ near 2300 MeV, two ${}^3P_2$ and two ${}^3F_2$ states, four 1^{--} states and two 0^+. We are able to identify all of these except for two 1^- states. It is hardly surprising that it is difficult to disentangle two states of low J^P.

3.1 Uniqueness

The ambiguities we have encountered concern signs of the amplitude ratios $r_4 =^3 H_4/{}^3F_4$ and $r_2 =^3 F_2/{}^3P_2$. These are the ratios of amplitudes after centrifugal barrier factors are factored out, i.e. they are asymptotic ratios as $s \to \infty$. We have located two solutions with similar χ^2, one with r_4 positive and the other with r_4 negative. They both contain the same resonances with similar masses and widths, and differ mostly in coupling constants. However, analysis of $\eta\pi^0\pi^0$ data [12,20] allows a clear distinction between these alternatives. Clebsch-Gordan coefficients in equns. (4) and (5) are such that positive r_4 requires dominance of $M = 1$ amplitudes for $f_4(2300)$. [Here M is the projection of the spin of the initial state along the beam direction; $M = 1$ corresponds to f_{+-} in the helicity basis]. This agrees with the $\eta\pi^0\pi^0$ analysis. Negative r_4 is rejected strongly by that analysis.

There is an argument concerning matrix elements for decay which supports this conclusion. For this high spin, the wave function of the resonance is peaked strongly at a radius of 0.8–1.0 fm. Wave functions for the $\bar{p}p$ channel are described by spherical Bessel functions. For momenta in the mass range under discussion, the first zero of $j_L(kr)$ lies outside 2 fm for both $L = 3$ and $L = 5$. Overlap of wave functions with the resonance leads to the expectation that $\bar{p}p$ ${}^3F_4$ and ${}^3H_4$ will couple to the resonance with the same sign, hence r_4 positive. We find that the fitted amplitude ratios $r_5 =^3 I_5/{}^3G_5$ and $r_3 =^3 G_3/{}^3D_3$ are likewise positive, as one would expect from the same argument.

We shall present evidence for four 2^+ resonances at 1910, 2020, 2230 and 2300 MeV. We shall argue for several reasons that the $f_2(2020)$ is the first $q\bar{q}$ ${}^3F_2$ state. We have examined all alternative sign combinations of r_2 for these four resonances. The $\pi^-\pi^+$ polarisation data are sensitive to these signs. The best solution is obtained with signs respectively +, +, -, - in the order $f_2(1910)$ to $f_2(2300)$. The second best solution has signs -, -, -, -, but a χ^2 of 13850, i.e. worse by 3265 than the best solution. The increase in χ^2 is mostly for polarisation data, where there is a clear systematic discrepancy between data and fit for the second alternative. For $f_2(2020)$, r_2 is again expected to be positive. The first zero of the Bessel function $j_1(kr)$ (coupling to ${}^3P_2$) again lies outside 2 fm; so the $\bar{p}p$ momentum is low enough that the argument given above remains unchanged.

For $f_2(2300)$, which we shall interpret as the radial excitation of $f_2(2020)$, the momentum in the $\bar{p}p$ channel is such that the first zero of $j_1(kr)$ lies at 1.28 fm. When one allows for (i) the fact that the wave function will be attracted to smaller r by the resonant interaction (mixing in a component due to the irregular function $n_1(kr)$), and (ii) the node in the radial wave function of the resonance, it is possible to arrive at a negative r_2, as observed. For $q\bar{q}$ ${}^3P_2$ states, it is not possible to make reliable predictions, because of the large number of nodes in the radial wave functions of the resonances. They are, however, found to show the same general variation with s as for other J^P, i.e. positive for low $\bar{p}$ momenta and going negative for high momenta.

3.2 Quality of the fit

A solution is obtained in typically 1-2 minutes of computing; consequently several thousand fits have been made, exploring the systematic effects of including or omitting various resonances. In the course of this work, we have found, from the observed variations from fit to fit, that errors on resonance masses and widths may be assigned from χ^2 changes of ~ 20. This is the quantitative criterion we adopt in assessing errors given here. It is larger than statistics ($\Delta\chi^2 = 1$) and therefore conservative. It covers almost all of the variations which have been observed between fits with differing ingredients; where it does not, errors have been increased to cover the observed variations.

The $\pi^0\pi^0$ data have statistical errors which are much smaller than those of other data. Consequently, there is the danger that delicate features of the $\pi^0\pi^0$ data cause problems in fitting other channels. To remedy this, we reduce the weight of the $\pi^0\pi^0$ data by a factor 3, and increase the weight of $\eta\eta'$ by a factor 2. This does not introduce any major qualitative changes, but speeds convergence greatly.

Values of χ^2 for all data sets are given in Table 1. They are somewhat above 1 per point, particularly for $\pi^0\pi^0$, because of the weighting mentioned above. It may reflect the presence of systematic errors in some data points, but also may reflect small missing components in the fit (e.g. backgrounds from the tails of lower mass resonances), which cannot presently be identified unambiguously. Our objective is to locate the essential features of the data, and these are stable against small variants in the parametrisation of the amplitudes.

Data	Author	Points	χ^2
$\pi^-\pi^+$	Hasan	1000	2677
P	Hasan	1000	1812
$\pi^-\pi^+$	Eisenhandler	960	1702
P	Eisenhandler	1078	1720
$\pi^0\pi^0$	Anisovich	360	1853
$\eta\eta$	Anisovich	360	667
$\eta\eta'$	Anisovich	144	142
Normalisations	Anisovich	27	12

Table 1: Contributions to χ^2 of the fit.

3.3 Normalisation

Each of the data sets on $\pi^0\pi^0$, $\eta\eta$ and $\eta\eta'$ is given a normalisation constant which has been determined in Ref. [1]. In our final fits, the normalisation is optimised by allowing each data set to vary in normalisation and including into χ^2 a contribution for the deviation of the normalisation from its experimental value.

As described in [1], the normalisation of Crystal Barrel data for $\pi^0\pi^0$ is on average slightly more than a factor 2 higher than that of data of Dulude et al. [21]. This calls into question the absolute normalisation of all the neutral data. In order to test this, we have tried scaling the normalisation of all Crystal Barrel data for $\pi^0\pi^0$, $\eta\eta$ and $\eta\eta'$ down by this factor 2, so as

to agree on average with Dulude et al. It results in a huge increase in χ^2 from 10585 to 16893. The polarisation data are particularly sensitive to this change, increasing from 3532 to 7940.

The reason for this is straightforward, but important. Partial waves in the $\pi^0\pi^0$ channel have isospin 0 and even spin. These amplitudes contributes also to $\pi^-\pi^+$ data, but interfere with $I = 1$ components with odd spin. This interference gives rise to forward-backward asymmetries in the differential cross section, depending on real parts of interferences. Values of $Pd\sigma/d\Omega$ contain interferences depending on imaginary parts of identical interference terms. The normalisation of Dulude et al. requires much larger $I = 1$ amplitudes than our data. A fit to the data of Dulude et al. alters the phases of interferences, in order to fit asymmetries in differential cross sections. But these changes are inconsistent with the polarisation data. This inconsistency rules out the normalisation of Dulude et al. If we float the normalisation of Crystal Barrel data freely, it optimises at 0.989 times the published values. An increase of χ^2 of 20 (the criterion we have adopted above in discussing resonance masses and widths) corresponds to a change of ± 0.023 in normalisation. This lies within the normalisation errors quoted for Crystal Barrel data, namely ± 0.03 for momenta of 1050 MeV/c upwards and ± 0.06 at 600 and 900 MeV/c.

In the final analysis, we do not use the factor 0.989. The normalisation of Crystal Barrel data is used with its experimental normalisation and with the errors (3–6%) obtained experimentally.

We include the data of Dulude et al. for the determination of the shape of the angular distribution. They provide some valuable points close to $\cos\theta = 1$. However, their normalisation is fitted freely.

3.4 Comparison of data and fit

Figs. 1–5 show comparisons of our final fit with data for $\pi^-\pi^+$ differential cross sections, polarisation and integrated cross sections. The $\pi^0\pi^0$ data, $\eta\eta$ and $\eta\eta'$ are available only up to centre of mass scattering angle θ given by $\cos\theta \leq 0.875$. Their integrated cross sections are therefore compared in Fig. 5 with the fit only over this angular range. The $\pi^-\pi^+$ data are available over the full angular range and are integrated over this range.

Panels on Figs. 1–3 labelled H refer to Hasan et al; those labelled E refer to Eisenhandler et al. or the same experiment of Carter et al. On Fig. 1, the angular distributions are mostly fitted well. There are small discrepancies near $\cos\theta$ = -1 for momenta of 790, 988, 1089, 1140, and 1291 MeV/c. However, in all cases, data from the other experiment at nearby momenta show either no discrepancy or small ones. We therefore take these discrepancies to be due to experimental error or statistics. There is some discrepancy with $d\sigma/d\Omega$ near $\cos\theta$ = -1 at 467,497 and 585 MeV. We can find no solution which resolves this discrepancy without rapid changes with mass in high partial waves $J = 4$, 5 or 6; at these momenta, contributions from $J = 5$ and 6 should be small.

On Fig. 2 there are some discrepancies at individual momenta, but nothing systematic over a range covered by a resonance. Above 2 GeV/c, we are fitting only with tails of resonances from lower masses, plus resonances with $J^P = 6^+$, 5^-, 4^+, and 2^+ in the range 2500–2600 MeV. It seems likely that there will be further low spin resonances in this mass range. We have tried adding one by one resonances with $J^P = 3^-$, 1^- and 0^+, but none gives a significant improvement in χ^2. For polarisation data on Fig. 3, the agreement between data and fit is generally satisfactory and free of systematic trends.

The fit to $\pi^0\pi^0$ data is shown in Fig. 4 and the accompanying paper on data analysis [1]. It

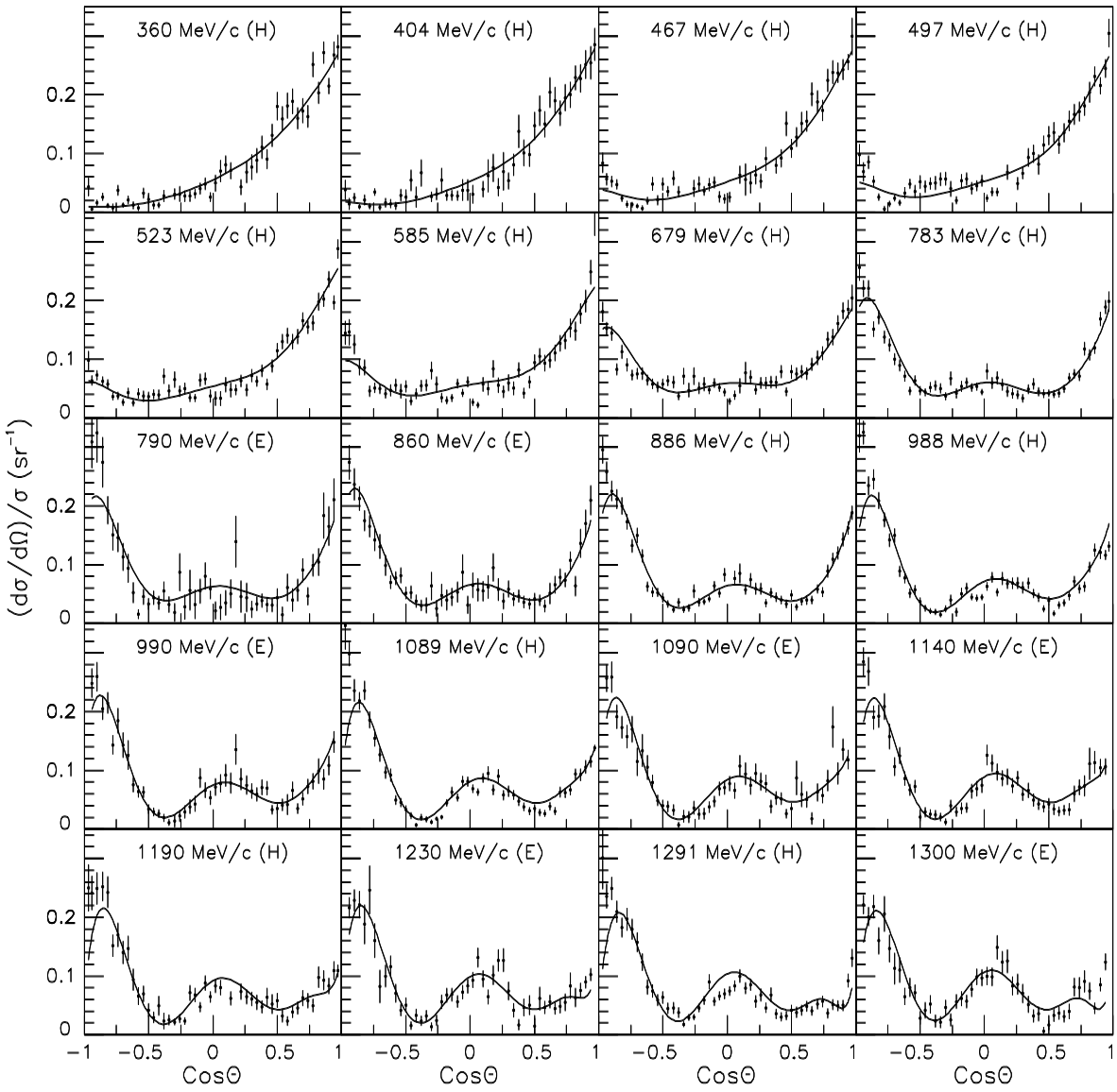


Figure 1: Differential cross sections from 360 to 1300 MeV/c, compared with the fit (full curves); panels labelled H are data of Hasan et al. and those labelled E are from Eisenhandler et al. Each distribution is normalised so as to integrate to 2π.

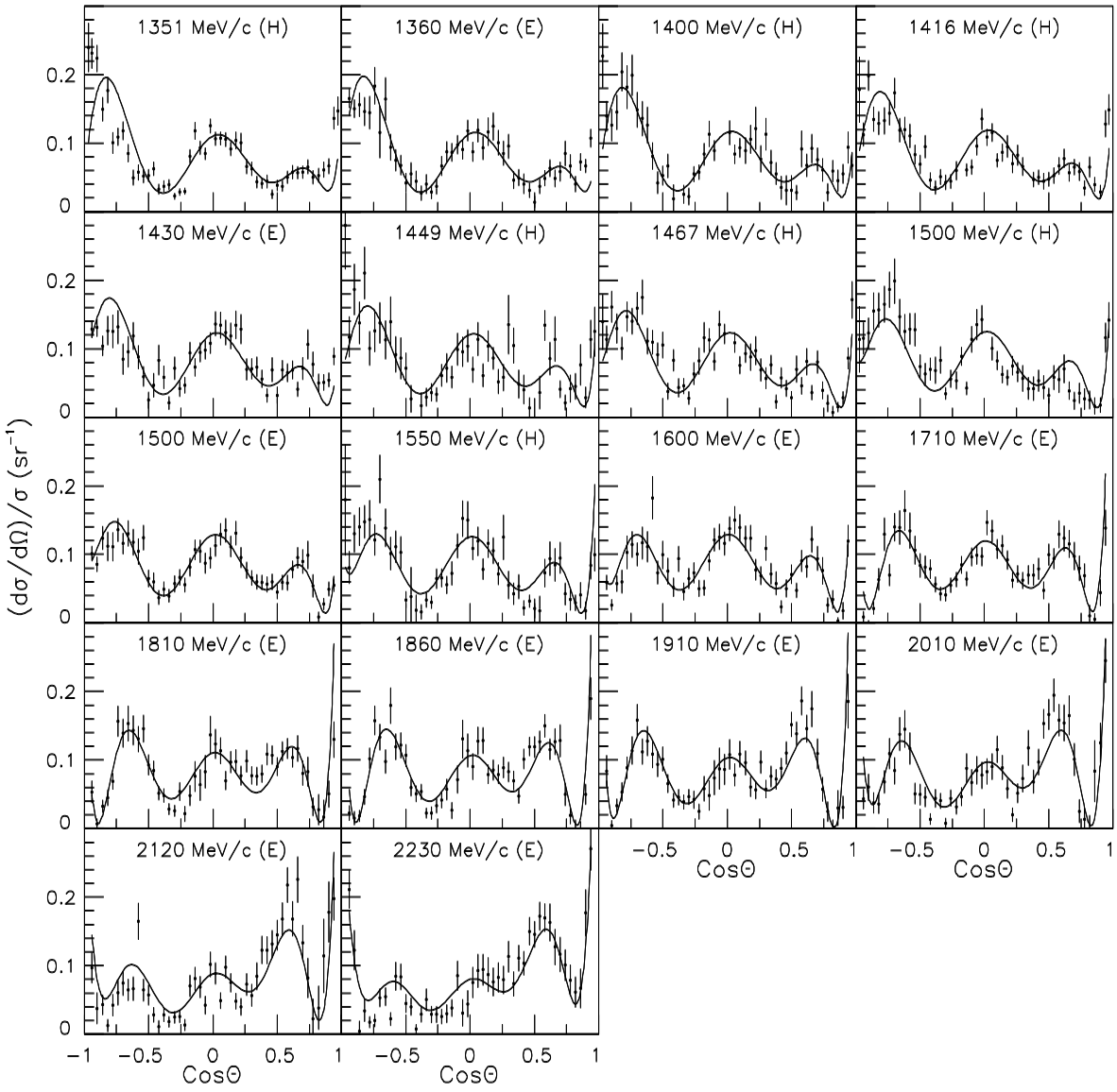


Figure 2: As Fig. 1, 1351 to 2230 MeV/c.

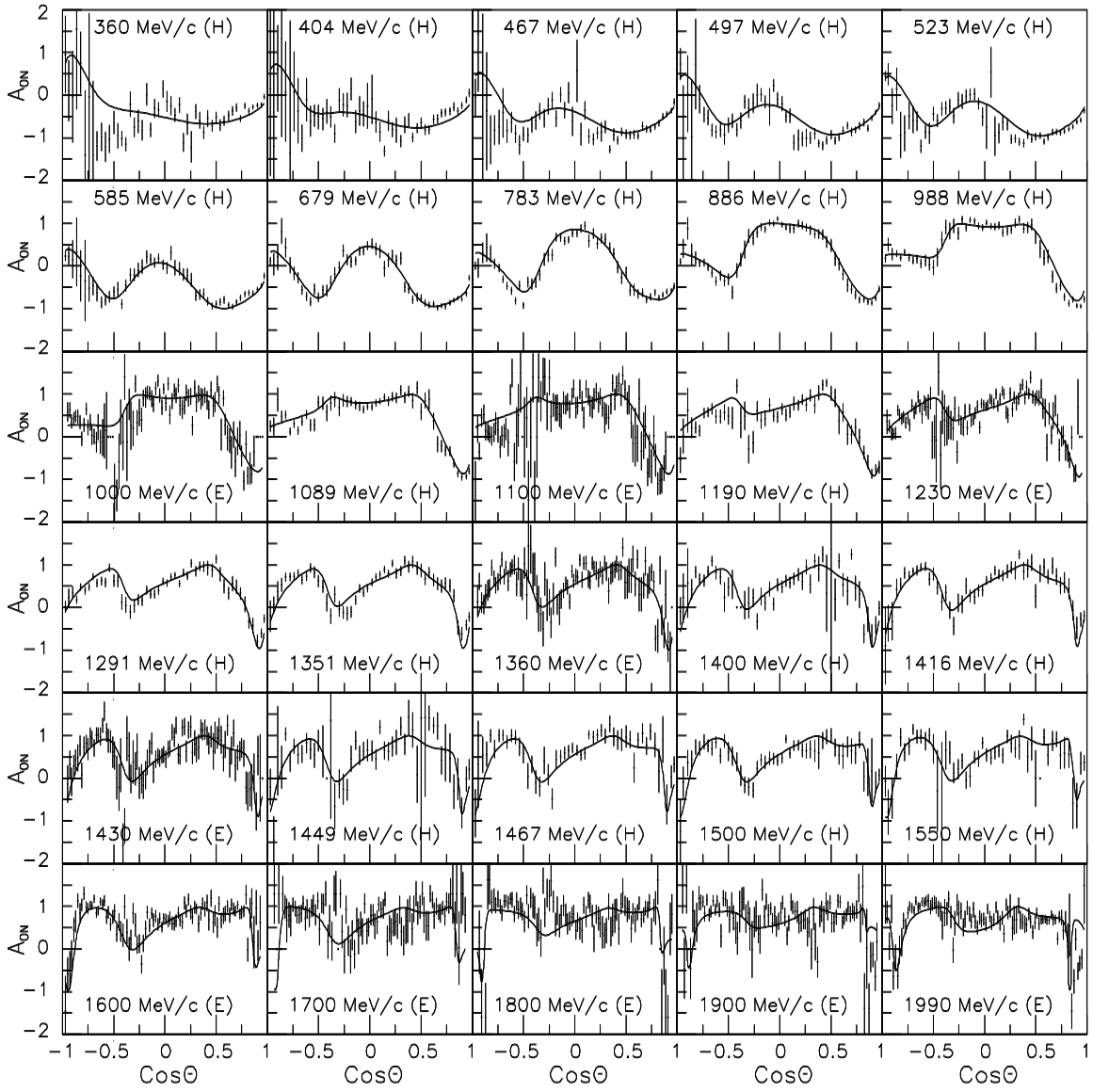


Figure 3: Polarisation data compared with the fit (full curves).

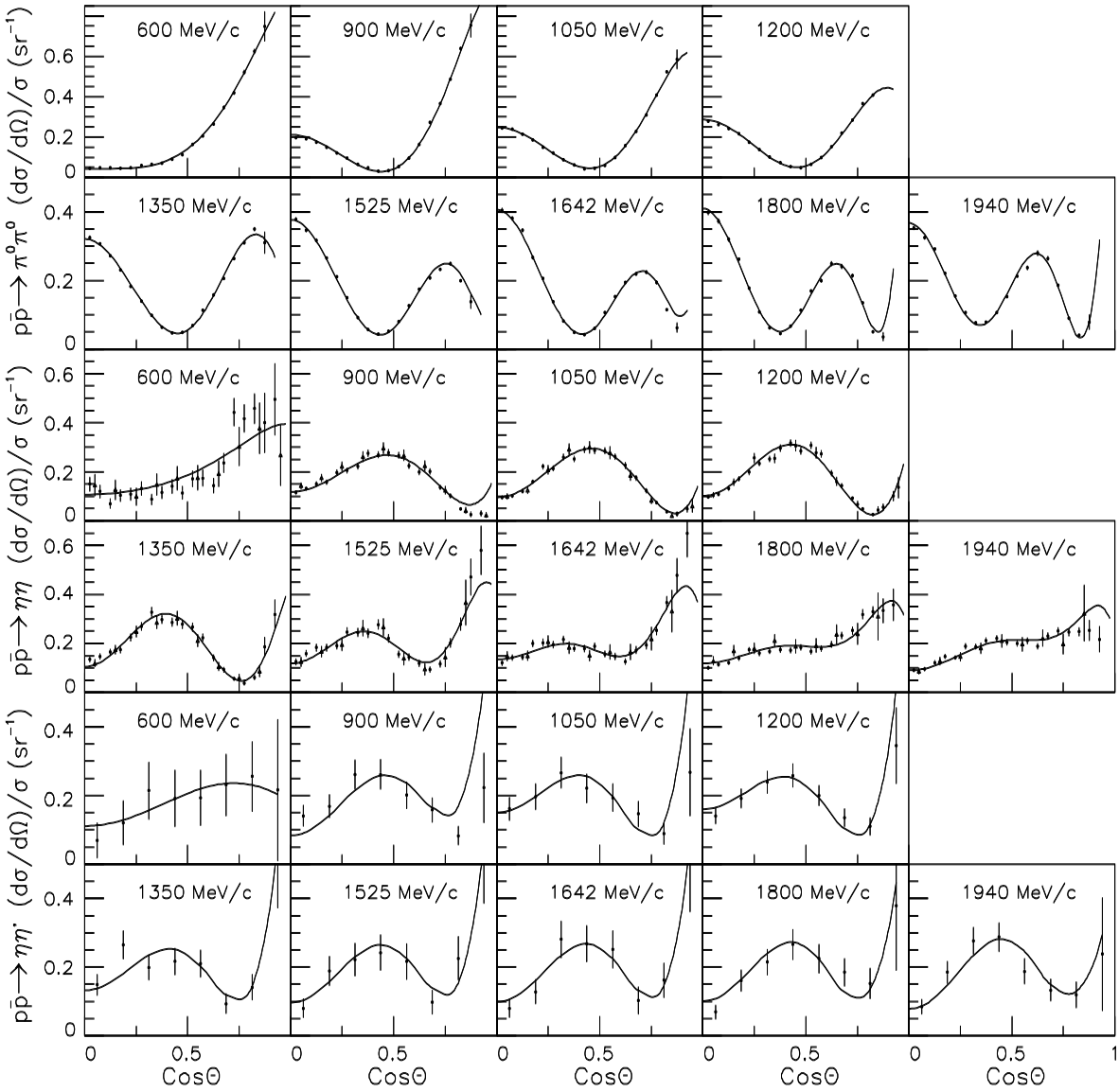


Figure 4: Differential cross sections for $\pi^0\pi^0$, $\eta\eta$ and $\eta\eta'$ compared with the fit (full curves). For $\eta\eta'$, these are the average of 4γ and 8γ data reported in Ref. [1].

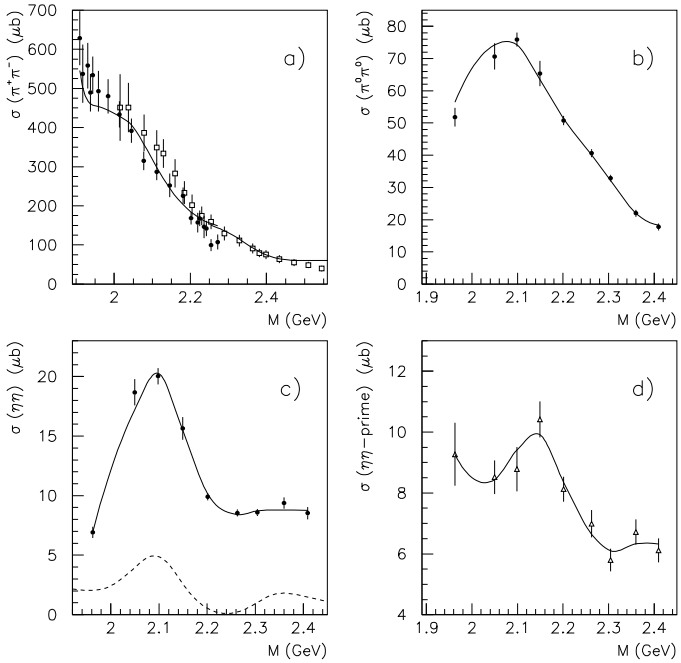


Figure 5: Integrated cross sections compared with the fit (full curves). For $\pi^0\pi^0$, $\eta\eta$ and $\eta\eta'$, the integration is from $\cos\theta = 0$ to 0.875 and is over only one hemisphere; the $\eta\eta'$ data are averaged over 4γ and 8γ data reported in Ref. 1. For $\pi^-\pi^+$ the integration is over the full angular range. In (a), black circles are data of Hasan et al. and open squares are those of Eisenhandler et al. The dashed curve in (a) shows the contribution from the 0^+ intensity.

is good at most momenta. At 1200 MeV/c, one point at $\cos\theta = 0.875$ cannot be fitted under any circumstances. The acceptance of the detector falls rapidly around $\cos\theta = 0.875$, so we suspect this point is affected by some systematic error. The data at 1200 MeV/c were actually taken in a run separate from all other momenta, possibly accounting for a discrepancy between this momentum and others.

For $\eta\eta$ data, shown on Fig. 4 and in the accompanying paper, the fit is generally good, though there are some discrepancies near $\cos\theta = 1$ at 900 and 1940 MeV/c. Fits to these regions may be improved by relaxing the constraints on phase angles ϕ_i. At 600 MeV/c, statistics are low and it is possible to obtain some variety of fits, varying the strengths of flavour mixing for $f_4(2020)$, $f_2(1910)$ and $f_2(2020)$. Near $\cos\theta = 1$, there is a dip in $\eta\eta$ differential cross sections at 900 MeV, but a peak at 600 MeV/c. Our fits are a compromise between these rapidly changing features. The fit to either momentum may be improved, but not both simultaneously. For $\eta\eta'$, fits are satisfactory, but statistics are low.

Integrated cross sections, shown on Fig. 5, are described well. For $\pi^0\pi^0$ in Fig. 5(b), the peak at 900 MeV/c is mostly due to $f_4(2020)$. For $\eta\eta$ in Fig. 5(c), the striking peak at 1200 MeV/c comes largely from $f_0(2105)$ and $f_4(2020)$.

3.5 Fitted Resonances

Fitted resonances are shown in Table 2. We shall comment in detail on most of them. All those in the mass range 1900–2400 MeV are established securely, with the exception of the 3^{--}

J^P	Mass M (Mev)	Width Γ (MeV)	$\Delta\chi^2$	Hasan M (MeV)	Hasan Γ (MeV)
6^+	2485 ± 40	410 ± 90	1776	-	-
5^-	~ 2500	~ 470	112	2881	310
5^-	2295 ± 30	235^{+65}_{-40}	2534	2303	169
4^+	~ 2500	~ 400	1305	2813	257
4^+	2300 ± 25	270 ± 50	2549	2314	278
4^+	2020 ± 12	170 ± 15	22382	(2049)	(203)
3^-	2300^{+50}_{-80}	340 ± 150	183	-	-
3^-	2210 ± 40	360 ± 55	368	2232	220
3^-	1960 ± 15	150 ± 25	2957	2007	287
2^+	~ 2620	~ 430	776	-	-
2^+	2300 ± 35	290 ± 50	2879	2517	264
2^+	2230 ± 30	245 ± 45	2290	2226	226
2^+	2020 ± 30	275 ± 35	2980	1996	134
2^+	1910 ± 30	260 ± 40	2286	-	-
1^-	2165 ± 40	160^{+140}_{-70}	450	2191	296
1^-	2005 ± 40	275 ± 75	1341	1988	244
1^-	(1700)	(180)	8444	(1690)	246
0^+	2320 ± 30	175 ± 45	1257	2321	223
0^+	2105 ± 15	200 ± 25	4030	2122	273
0^+	2005 ± 30	305 ± 50	370	-	-
0^+	(1700)	1000	2844	1745	238

Table 2: Resonances fitted to the data; errors cover the full range of systematic variations observed in a large variety of fits with varying ingredients. Values in parentheses either lie outside the range of masses fitted and describe background amplitudes or are fixed. The fourth column gives changes in χ^2 when each resonance is removed from the fit and all other parameters are re-optimised. The final two columns compare with results of Hasan and Bugg, Ref. [9].

resonance at 2300 MeV, which is rather weak. The fourth column of the table shows changes in χ^2 when each resonance is removed from the fit and all other parameters are re-optimised; this measures the significance of each contribution in fitting the data. Most of these changes are enormous and leave no possible doubt about the presence of these resonances. Our impression, from the consistency between alternative fits with differing ingredients, is that any resonance contributing a change in $\chi^2 > 100$ is definitely present. However, below $\Delta\chi^2 = 300$, the mass and particularly the width are hard to establish with confidence. Those resonances contributing 1000 to the improvement in χ^2 are very secure in all parameters.

Argand diagrams are shown for $\pi\pi$ amplitudes on Fig. 6 and those for $\eta\eta$ and $\eta\eta'$ on Fig. 7. Resonance loops are observed in all partial waves. We shall comment in detail later. Intensities of all partial waves are displayed in Fig. 8. Dashed contributions are for $L = J - 1$ and dotted for $L = J + 1$. [Interferences disappear from their sum].

There is a strong 4^+ resonance at 2020 MeV and a somewhat weaker, but definite, one at 2300 MeV; there is tentative evidence for another around 2500 MeV. A strong 5^- state is observed at 2295 and there is tentative evidence for a higher one at ~ 2500 MeV. There is definite evidence for the expected 6^+ resonance at 2485 ± 40 MeV. For $J^P = 3^-$, there are two well defined $^3D_3$ states at 1960 and 2210 MeV. There is tentative evidence for a further $^3G_3$ state at 2300 MeV, but it is weak; despite this, its angular dependence is distinctive and it is hard to avoid the conclusion that it is present, even if its mass and width cannot be determined well.

An important result is that there are definitely four 2^+ states at 1910, 2020, 2230 and 2300 MeV; these are expected from the quark model for $^3P_2$ and $^3F_2$. For $J^P = 1^-$, four states are again expected. There is evidence that two are required, and there are tentative indications of a third; however, it is not possible to establish the mass and width of this third state. For $J^P = 0^+$, at least two resonances are definitely required. The one at 2105 MeV appears very strongly, particularly in the $\eta\eta$ data, and its mass and width are determined precisely. There is a further definite 0^+ resonance at 2320 MeV. As we shall comment below, there is probably a third 0^+ state at 2005 MeV, but its mass and width are not well determined because of overlap and interference with $f_0(2105)$. We now discuss each resonance in turn, starting with the high mass region.

3.6 The mass range 2500–2600 MeV

Our main objective is to study the momentum range up to 1940 MeV/c, where the extensive Crystal Barrel data are available. However, we also fit the momentum range above 2 GeV/c with the objective of obtaining a reliable determination of the the tails of the high mass resonances below 2 GeV/c. The $\pi^-\pi^+$ differential cross section data extend to 2430 MeV/c and polarisation data to 2200 MeV/c.

We find definite evidence for a 6^+ resonance at 2485 MeV, in close agreement with the result of the GAMS collaboration [19]. Its contribution to χ^2 is large, as one sees from Table 2. We find it desirable to introduce further high mass contributions for 5^-, 4^+, and 2^+, as one sees from the changes they introduce into χ^2, listed in Table 2. However, only the lower half of each resonance is within the available mass range. The result is, of course, a strong correlation between fitted mass and width, so we are unable to assign accurate parameters to these resonances. Furthermore, masses of the high spin states are again sensitive to the radius of the centrifugal barrier.

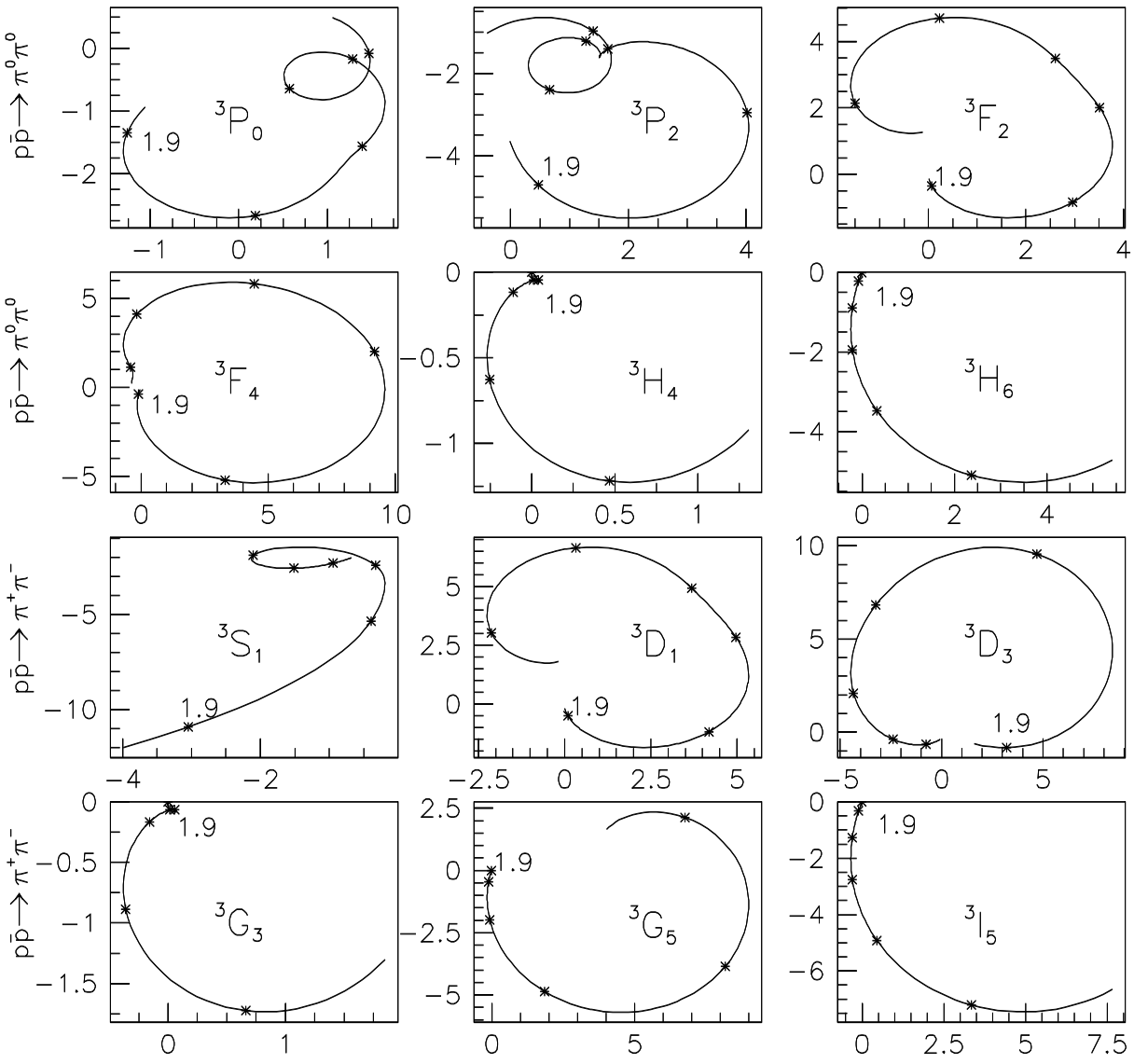


Figure 6: Argand diagrams for $\pi^+\pi^-$ partial wave amplitudes $f_J(s)$. Crosses mark masses at 100 MeV intervals beginning at 1900 MeV. The scale is such that the integrated partial wave cross section in given in μb by $2\pi|f_J(s)|^2\rho(s)$, where $\rho(s)$ is the phase space $q/\sqrt{s}$.

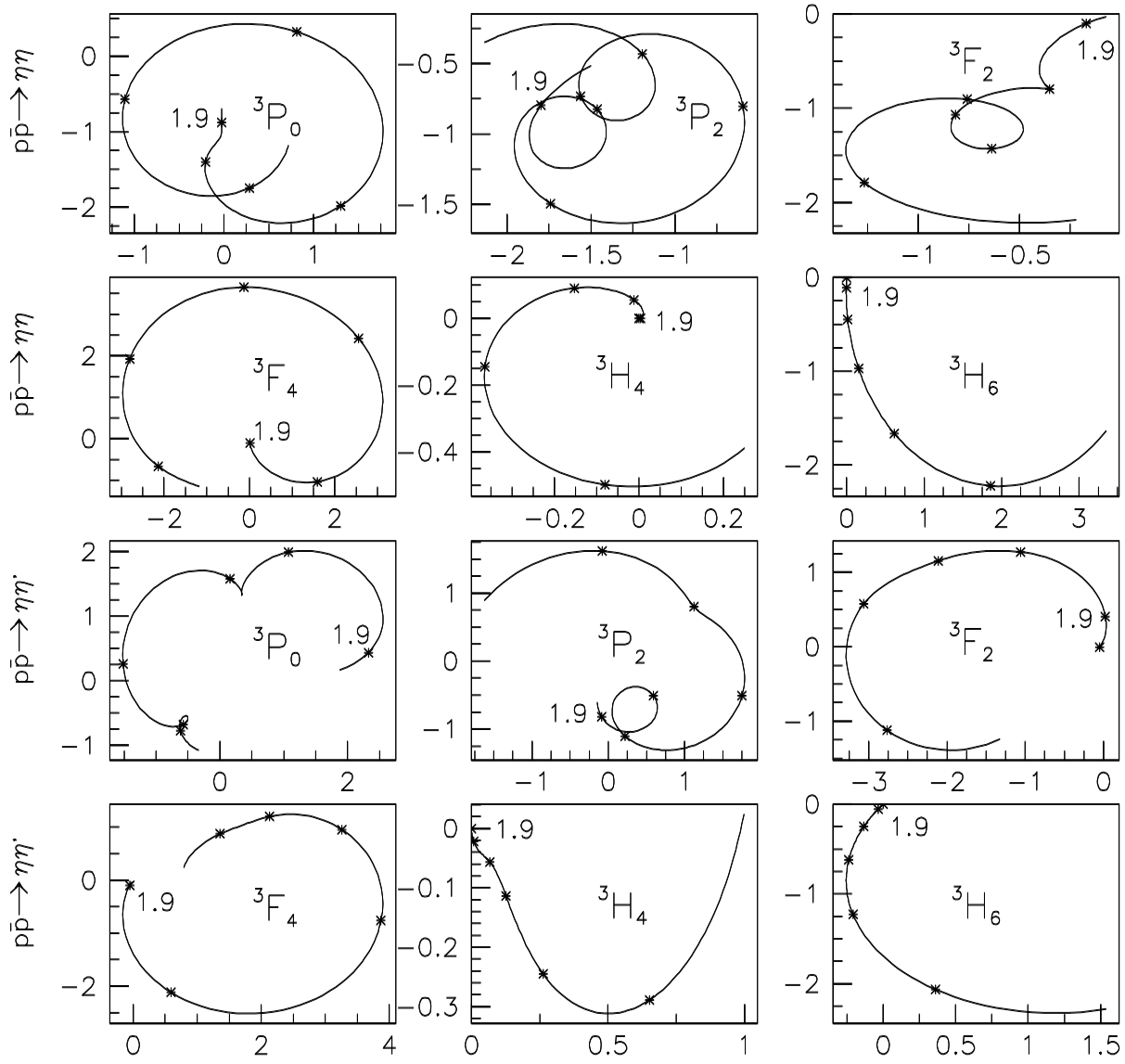


Figure 7: Argand diagrams for $\eta\eta$ and $\eta\eta'$ amplitudes. Crosses mark masses at 100 MeV intervals beginning at 1900 MeV. The scale is as described for Fig. 6.

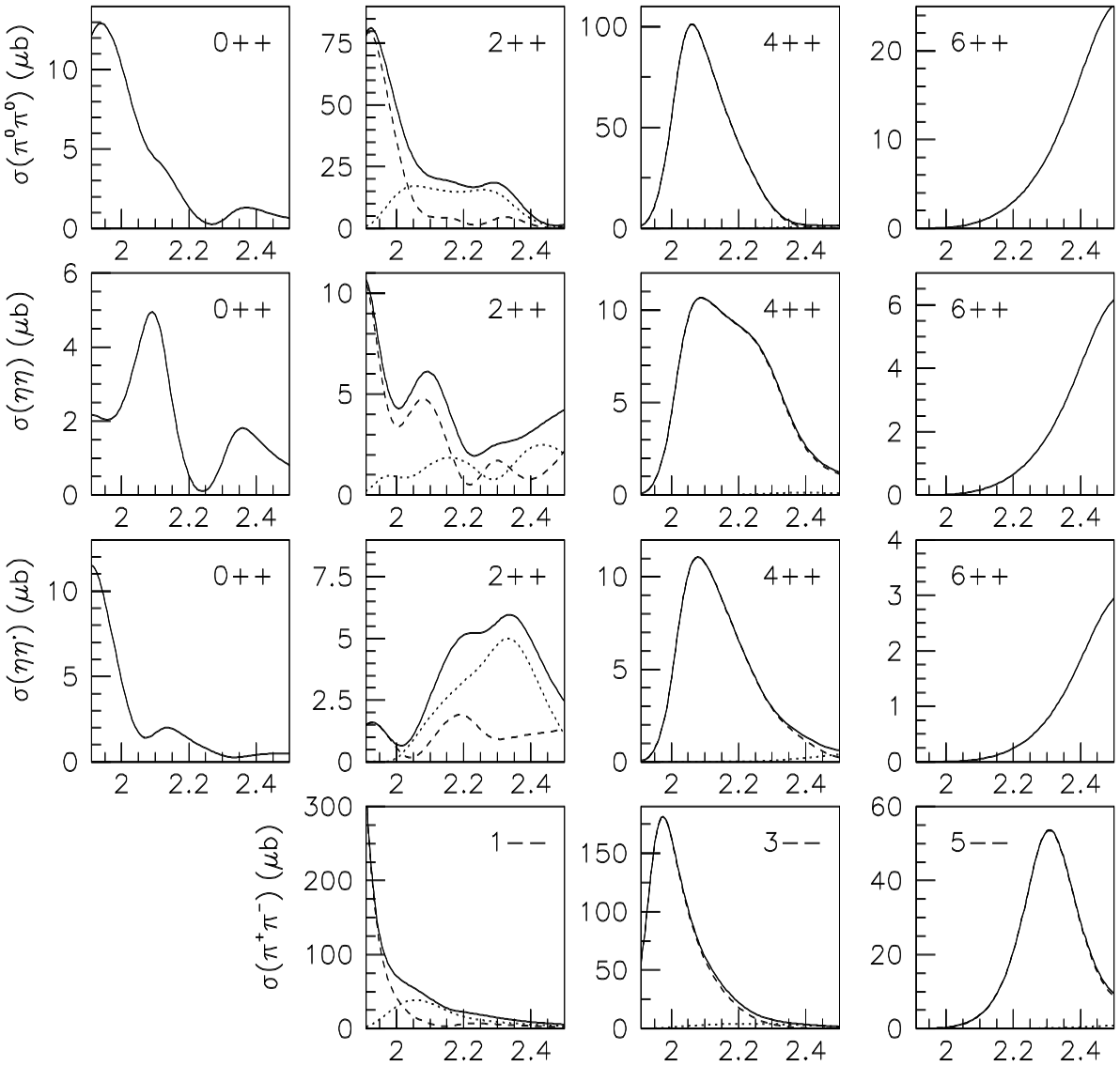


Figure 8: Intensities from individual J^P for channels $\pi^0\pi^0$, $\eta\eta$ and $\eta\eta'$. Dashed curves show contributions with $J = J - 1$ and dotted curves those with $L = J + 1$.

We now comment on individual resonances and illustrate on Fig. 9 the deterioration in the fit when they are dropped from the fit.

3.7 5^- and 4^+

The 5^- resonance at 2295 MeV is very clear in polarisation data. Figs. 9 (a)-(c) illustrate the deterioration in fits when it is removed. The width of $\rho_5(2295)$ is 235^{+65}_{-40} MeV, somewhat less than the 400 MeV quoted by the GAMS collaboration [22]. However, an inspection of the GAMS data reveals the possibilty that they have fitted resonances at 2295 and 2500 MeV by a single resonance. On Fig. 6 one sees that the 5^- state at 2295 MeV is dominantly $^3G_5$ and the well known $f_4(2020)$ is almost purely $^3F_4$. The centrifugal barriers for $\bar{p}p$ will suppress higher L strongly.

The phase advance of 360° for $^3F_4$ on Fig. 6 requires the presence of two 4^+ resonances. A second one at 2300 MeV is definitely required, but is fairly weak in the $\pi\pi$ channel, leading to a large uncertainty on its width. It is more clearly visible in $\eta\eta$ data. Earlier fits to $\pi\pi$ data [5–10] all gave masses in the range 2300–2340 MeV. Crystal Barrel data on the $\eta\pi^0\pi^0$ final state show a strong peak in $f_2(1270)\eta$ at 2320 ± 30 MeV with $\Gamma = 220 \pm 30$ MeV [12]. Also recent VES data display conspicuous 4^+ peaks in $\omega\omega$ at 2325 ± 15 MeV with $\Gamma = 235 \pm 40$ MeV [23] and in $\eta\pi\pi$ data with $M = 2330 \pm 10(stat) \pm 20(syst)$ MeV with $\Gamma = 235 \pm 20 \pm 40$ MeV [24].

3.8 3^{--} states

The 3^- state at 1960 MeV is strong and very secure. Statistically, the error on the mass is ±7 MeV and on the width is ±14 MeV. In all fits, it never moves outside the mass range 1950–1980 MeV. We increase errors to cover all systematic variations. An interesting point is that this resonance is definitely lower in mass than the corresponding 4^+ states. This demonstrates that all resonances in this region are not degenerate in mass. Again, the phase advance of 360° for $^3D_3$ on Fig. 6 requires the presence of at least two resonances. The higher one agrees well in mass with the determination of Hasan and Bugg, namely $M = 2232$ MeV. Both resonances are coupled dominantly to $\bar{p}p\ ^3D_3$.

In order to demonstrate that the data really demand the presence of each of these resonances, we have dropped them one by one from the fit and examined the discrepancies which emerge between data and fit. Figs. 9 (d) and (e) illustrate some of the defects when the lower 3^- resonance is dropped; Figs. 9(f) and (g) show defects in the fit when the upper 3^- resonance is removed. In both cases, there is a tendency for the remaining resonance to become broad and span the mass range.

A further $q\bar{q}\ ^3G_3$ state is expected in the mass range around 2300 MeV, close to $^3G_5$. There is evidence for its presence as $\rho_3(2300)$ of Table 2. However, it improves χ^2 only by 183, with the consequence that its mass and particularly its width are not well determined. It appears almost purely in $\bar{p}p\ ^3G_3$. The angular dependence of this state is distinct from $^3D_3$, making its presence very likely, despite the fact that its parameters are not well determined. This angular component requires a mass ~ 100 MeV above that of $\rho_3(2210)$.

We have also tried including $\rho_3(1690)$ as a background amplitude. It has only a very marginal effect, so we omit it. The reason may well be that it is inhibited near the $\bar{p}p$ threshold by the $L = 2$ centrifugal barrier.

3.9 2^+ states

An important outcome of the present analysis is strong evidence for four 2^+ states in this mass range, as expected from $q\bar{q}$ $^3P_2$ and $^3F_2$. Earlier, there has been evidence from VES and GAMS groups for an $f_2(1920)$ of rather narrow width, $\Gamma \simeq 90$ MeV [25,26]. Recent VES data on $\omega\omega$ give an improved mass determination of 1937 ± 12 MeV and width $\Gamma = 150 \pm 17$ MeV [23]. Data on $\eta\pi^0\pi^0$ from Crystal Barrel [12,20] require 2^+ states at (a) M$= 2020 \pm 50$ MeV, $\Gamma = 200 \pm 70$ MeV, decaying dominantly to $f_2(1270)\eta$, (b) $M = 2240 \pm 40$ MeV with $\Gamma = 170 \pm 50$ MeV, appearing as a second peak in $f_2(1270)\eta$, and (c) $M = 2370 \pm 50$ MeV with $\Gamma = 320 \pm 50$ MeV, appearing as a strong peak in decays to $a_2(1320)\pi$.

The inclusion of polarisation data is important in clarifying the components required in the fit. The $f_2(1920)$ appears very strongly with $M = 1910 \pm 30$ MeV, $\Gamma = 260 \pm 40$ MeV. However, it is at the bottom end of the range of data we analyse, and we observe some tendency for its mass to drift downwards. We view the determination of the mass by VES and GAMS as more secure, but our larger width appears reliable. If this resonance is dropped from the fit, χ^2 increases by a definitive amount, namely 2290. There are large effects on the fit at many of the low momenta; effects at two momenta are illustrated in Figs. 9(j) and (k).

The next 2^+ state optimises at 2020 ± 30 MeV with $\Gamma = 275 \pm 35$ MeV. In earlier fits to $\eta\pi\pi$ data [12] there is the possibility of cross-talk between the two nearby resonances at 1910 and 2020 MeV, both lying at the bottom end of the available mass range in the neutral data. So the confirmation of $f_2(2020)$ is important. We find a very large change in χ^2, namely 2980, when $f_2(2020)$ is removed from the fit and others are re-optimised. Figs. 9(l) and (m) illustrate the deterioration in the fit to some data.

The present analysis confirms the presence of two further 2^+ states at 2230 MeV and 2300 MeV. When the resonance at 2230 MeV is removed and others are re-optimised, χ^2 gets worse by 2290, a very large amount. The effect of removing it is to produce a fit with a single resonance at 2280 MeV. The effect of removing the highest 2^+ state at 2300 MeV is 2879 in χ^2. Again the effect is to move the 2230 MeV resonance close to 2280 MeV and produce the same bad fit as is illustrated in Figs 9(n) and (o).

The highest of these f_2 states, now at 2300 ± 30 MeV, was observed in Refs. [12] and [20] at 2370 ± 50 MeV. This shift in mass arises from a subtle interference with $f_2(2230)$, revealed by the $\pi^-\pi^+$ polarisation data. For the same reason, the width of the $f_2(2230)$ is now 245 ± 45 MeV, rather than the 170 ± 50 MeV reported earlier.

All four states appear to be dominantly $q\bar{q}$. We shall discuss below the flavour mixing angles.

3.10 1^- states

The fit is poor without two 1^- resonances. The phase advance for $^3D_1$ on Fig. 6 is evidence for the presence of two states. However, four are to be expected in this mass range, originating from $\bar{p}p$ $^3S_1$ and $^3D_1$. We cannot identify more than two with confidence.

Figs. 9(h) and (i) illustrate the effect of dropping the 1^- state at 2000 MeV and re-optimising the rest. There are significant visible discrepancies in fits to both diffential cross sections and polarisation at low momenta. The change in χ^2 is 1341. It couples strongly to $\bar{p}p$ $^3D_1$ and this makes it distinctive in polarisation data in the low momentum range where $^3S_1$ dominates. The 1^- state at 2165 MeV has a less significant effect, improving χ^2 by only 450. It couples

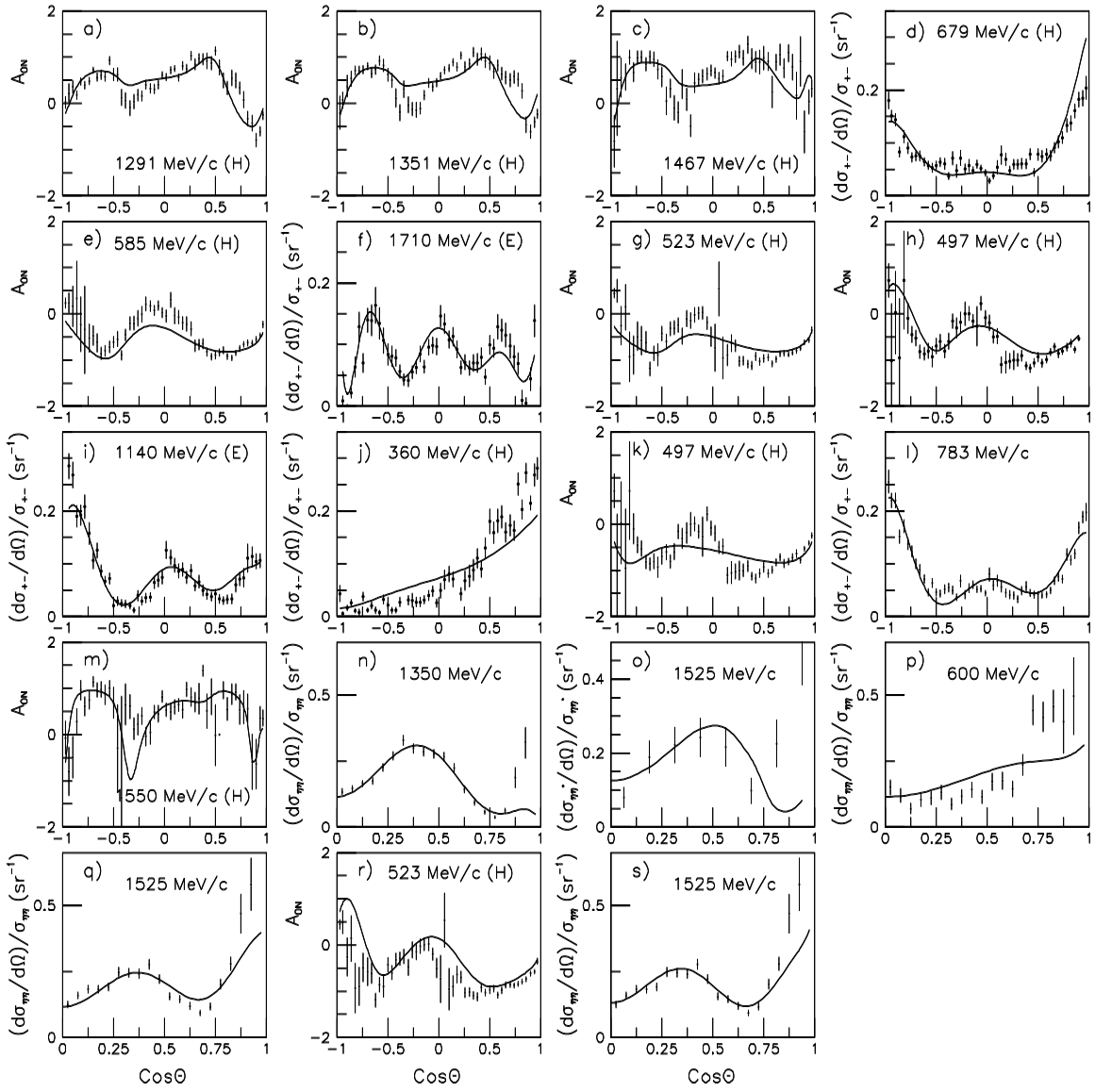


Figure 9: Illustrating the deterioration in the fits to data when various resonances are dropped from the fit: (a)–(c) $\rho_5(2295)$, (d)–(e) $\rho_3(1960)$, (f)–(g) $\rho_3(2210)$, (h)–(i) $\rho_1(2005)$, (j)–(k) $f_2(1910)$, (l)–(m) $f_2(2020)$, (n)–(o) $f_2(2230)$ or $f_2(2300)$, (p)–(r) $f_0(2105)$ and (s) $f_0(2320)$.

dominantly to $\bar{p}p\ ^3S_1$. When it is removed from the fit, changes are just discernible by eye. There are, however, reports of a 1^- resonance at 2150 MeV from GAMS data on the $\omega\pi$ channel [22]. This mass corresponds closely to what we observe. The width given by GAMS is large, 320 ± 70 MeV. The width we observe is smaller, but has a considerable error, 160^{+140}_{-70} MeV, so there is no discrepancy.

We find it is also essential to include a strong 1^- contribution peaking at or below the $\bar{p}p$ threshold. It fits well as a contribution from $\rho(1700)$. It is possible that some of this effect originates from the $^3S_1$ threshold in $\bar{p}p$, but a fit using only this threshold is somewhat poorer.

We have searched for further 1^- resonances at higher mass. There is some improvement in χ^2, with an additional state around 2270 MeV. However, the analysis will not support the presence of three 1^- states.

3.11 0^+ states

One of the very striking features of the $\eta\eta$ data is a strong peak in the integrated cross section of Fig. 5(c) at 2100 MeV. It is not fitted by $f_4(2020)$ and $f_2(2020)$, whatever the centrifgual barrier radius. These states with non-zero spin are separated by their characteristic angular dependence, despite possible interferences between them. The data demand very strongly the presence of an f_0 with mass 2105 ± 15 MeV. When it is dropped from the fit, χ^2 gets worse by a very large amount, namely 4030. The description of the integrated $\eta\eta$ cross section is then much worse, and there are also discrepancies with $\eta\eta$ differential cross sections, illustrated with examples in Figs. 9(p)–(r). This resonance has the best determined mass and width of all the resonances observed in the present analysis, except for $f_4(2020)$.

The mass agrees well with that observed by the E760 group [27] as a strong peak in $\eta\eta$ in the reaction $\bar{p}p \to \eta\eta\pi^0$ at two beam momenta of 3.1 and 3.5 GeV/c. The width we fit here, namely 200 ± 25 MeV, is close to that fitted by E760: 203 ± 10 MeV. These parameters also agree well with the mass fitted to a 0^+ peak in the 4π channel in $J/\Psi \to \gamma(4\pi)$ [28]. This resonance has also been identified as having $J = 0$ in an analysis of Crystal Barrel data on $\bar{p}p \to \eta\eta\pi^0$ [29], where it appears as a strong peak in $\eta\eta$; there, the determination of mass and width were not so precise, since the resonance appears at the top end of the available phase space. It is presently incorrectly listed by the Particle Data Group under $f_2(2150)$.

We find a strong requirement for a further 0^+ resonance at 2320 MeV. If it is omitted, the fit gets visible worse, as is illustrated in Fig. 9(s); χ^2 increases by 1257, a highly significant amount.

There has been a report of a further 0^+ resonance at 2020 MeV with a width of 400 MeV [30]. Adding this resonance to the fit, χ^2 improves by 370, which we regard as significant. However, because it lies towards the bottom end of the available data for $\pi^0\pi^0$ and $\eta\eta$ and because of interference with $f_0(2105)$, its mass and width have sizeable errors, $M = 2005 \pm 30$ MeV, $\Gamma = 305 \pm 50$ MeV.

4 Systematics of resonances masses

On Fig. 10(a), we plot mass squared of 2^+ resonances against their recurrence number. It is possible to construct an almost straight line from $f_2(1270)$, $f_2(1565)$, $f_2(1910)$ and $f_2(2230)$.This

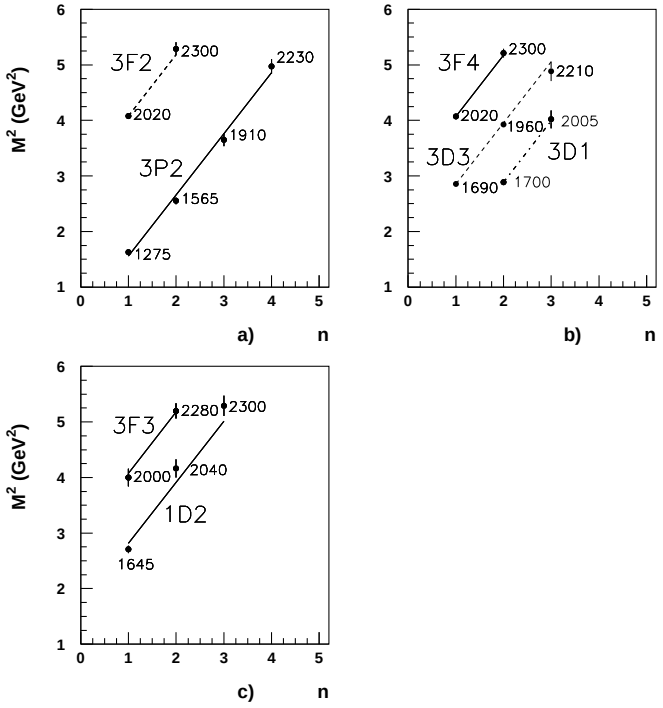


Figure 10: (a) Suggested trajectories for ${}^3P_2$ states (full line) and ${}^3F_2$ (dashed) v. radial quantum number n; (b) likewise for 4^+ states (full line), 3^- (dashed) and 1^- (dotted); (c) trajectories for 3^+ and 2^- states. Numerical values give masses in MeV.

is illustrated by the full line on Fig. 10(a). We make use of one result as yet unpublished [31]. The mass of the $f_2(1565)$ has been obtained from an analysis of Crystal Barrel data on $\bar{p}p \to \omega\omega\pi^0$ at rest. From a fit with a Flatté form, the K-matrix mass is determined to be $1598 \pm 11(stat) \pm 9(syst)$ MeV.

The $f_2(2020)$ and $f_2(2300)$ are readily placed on a parallel trajectory, shown by the dashed line of Fig. 10(a). The proximity of the $f_2(2020)$ to $f_4(2020)$ then suggests strongly that it is the $q\bar{q}$ ${}^3F_2$ $n = 1$ state and the $f_2(2300)$ is its radial excitation. The states on the full line of Fig. 10(a) are naturally interpreted as $q\bar{q}$ ${}^3P_2$ states. We interpret the shift in mass between the two lines as originating from the centrifugal barrier in the $q\bar{q}$ system. This provides an effective repulsion at small radii which shifts the resonance mass up more for $L = 3$ (${}^3F_2$) than $L = 1$ ${}^3P_2$.

The slopes of the lines on Fig. 10(a) are 1.10 GeV^2, with an error of ± 0.03 GeV^2. We find that it is possible to construct similar trajectories of identical slope for other quantum numbers. Fig. 10(b) shows corresponding trajectories for 4^+, 3^- and 1^- states. There is a well defined shift in mass between $\rho_3(1960)$ and $f_4(2020)$, which may again be attributed to the effect of the centrifugal barrier, namely 50–60 MeV per unit of L. The dotted line on Fig. 10(c) shows a possible trajectory made up of $\rho(1700)$ and $\rho(2005)$.

For $J^P = 2^-$, there is some indication of a discrepancy with a straight trajectory. However, there is evidence for an extra state $\eta_2(1875)$ [32]. If all these 2^- states are confirmed, this is likely to be an intruder state. It has a mass roughly that expected for a 2^- hybrid [33].

From the analysis of $\eta\pi^0\pi^0$ data, we can identify corresponding trajectories for $I = 0$ $q\bar{q}$ 3^+

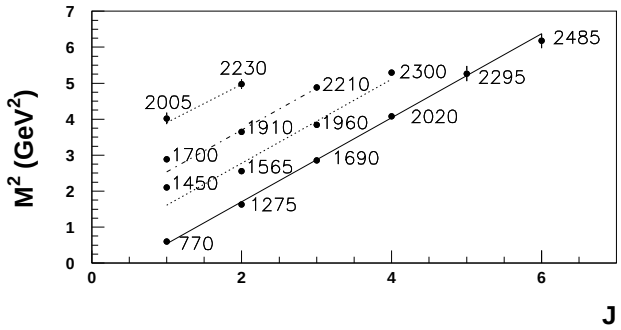


Figure 11: Regge trajectories for mesons with spins 1 to 6. Numerical values give masses in MeV.

and 2^- states. They are shown on Fig. 10(c). For 3^+, they are compatible with a trajectory of the same slope as other J^P on Fig. 10, and with $^3F_3$ states approximately degenerate with $^3F_4$ and $^3F_2$. The assignment of 0^+ resonances is presently controversial, so we do not show a trajectory for 0^+.

Fig. 11 shows Regge trajectories. The leading trajectory made up of $\rho(770)$, $f_2(1270)$, $\rho_3(1690)$, $f_4(2020)$, $\rho_5(2295)$ and $f_6(2485)$ is well known. These resonances lie close to a straight line versus s of slope 1.18 GeV^2 per unit of spin. One can just discern a possible slight difference (~ 0.1 GeV^2) between the trio 1^-, 3^- and 5^- and the even spin states. The slope is significantly greater than that of the lines on Fig. 10. Proof of this is the mass difference between $f_4(2020)$ and its grand-daughter $f_2(1910)$, likewise between $\rho_5(2295)$ and $\rho_3(2210)$ and the very clearly determined difference between $f_4(2020)$ and $\rho_3(1960)$. The centrifugal barrier in the $\bar{q}q$ system provides an explanation why high J states move up in mass. The intercept at zero mass with the vertical axis is at -0.67, slightly lower than the accepted value of -0.55 deduced from πN scattering data [34]; however, the systematic shift between even and odd spins on this trajectory allows the possibility of moving the intercept up by 0.1.

Fig. 11 also shows further parallel Regge trajectories. It is interesting that $\rho(1700)$ and $\rho(1450)$ depart significantly from straight-line trajectories through states of higher spin. Donnachie and Clegg [35] have argued that decay modes of $\rho(1450)$ require it to be a hybrid or mixed with a hybrid.

5 Flavour mixing

We have explained in section 2 that there is a blurred distinction between (i) allowing phases ϕ_i of decay channels to vary from 0 or (ii) allowing flavour mixing through the angles Φ. Nonetheless, we feel it is worth summarising the fitted values of flavour mixing angles Φ for 2^+ and 4^+ states. These are shown in Table 3. Errors on individual flavour mixing angles are typically $\pm 5^\circ$. However differences in Φ between different resonances are strongly correlated. These differences are what allow an acceptable fit to the data via small deviations from SU(3). Nonetheless some flavour mixing is inevitable. If they are all set to zero, there is an unacceptable increase of 2646 in χ^2.

Table 3 also includes fitted values of corresponding ratios r of amplitudes for spins 1, 3,4

and 5. Errors are typically ±15%. One discerns a trend from positive values for low masses to negative values at high masses. As the mass rises, the momentum in the $\bar{p}p$ channel increases and the first zero of $j_L(kr)$ describing the $\bar{p}p$ channel moves to smaller radius. As it moves inside the radius where the resonance wave function peaks, one expects a change of sign of the ratios of amplitudes r between $L = J \pm 1$, in qualitative agreement with the observations. However, because high mass resonances have several nodes in the wave function of the resonance, it is difficult to be quantitative for $J^P = 2^+$ and 1^- states at present.

Resonance	$\Phi(^\circ)$	r_J
$f_2(1910)$	1.1	2.89
$f_2(2020)$	7.9	1.62
$f_2(2230)$	7.5	-0.38
$f_2(2300)$	-14.8	-0.92
$f_2(2620)$	(0)	-0.83
$f_4(2020)$	-26.1	0.04
$f_4(2300)$	22.9	0.35
$\rho_5(2295)$		(0)
$\rho_5(2500)$		0.24
$\rho_3(1960)$		0.04
$\rho_3(2210)$		0.35
$\rho_3(2300)$		2.0
$\rho_1(2005)$		5.0
$\rho_1(2165)$		-0.22

Table 3: Values of flavour mixing angles Φ and ratios of amplitudes $r_J = |f_{L=J+1}|/|f_{L=J-1}|$ as $s \to \infty$.

A possibility is that the flavour mixing arises purely from the overlap with neighbouring $s\bar{s}$ states. The $s\bar{s}$ partner of $f_2(1565)$ could be the 2^+ state reported by the LASS group at 1950 MeV [36] decaying to $K^*\bar{K}^*$, in which case mixing with $f_2(1910)$ would be natural. On the other hand, the LASS group may simply be observing the decays of $f_2(1910)$. The $s\bar{s}$ partner of $f_2(1910)$ itself is expected around 2150–2250 MeV. It is possible to identify the states observed in $\phi\phi$ as the $s\bar{s}$ partners of $f_2(1910)$ and $f_2(2020)$. The 2^+ state decaying to the $\phi\phi$ S-wave, reported by Etkin et al. [37], also peaks at about 2150 MeV; however, their K-matrix analysis assigns it a mass of 2020 MeV, because of a strong threshold effect. The JETSET group have likewise reported a signal in $\bar{p}p \to \phi\phi$ peaking at $\sim$ 2180 MeV, possibly the same object [38]. Prokoshin has reported a peak in $\eta\eta$ at 2175 ± 20 MeV [39], again possibly the same resonance. Recent data of the Omega group on central production of K^+K^- reveals a peak at 2150 MeV [40].

Etkin et al. have also reported a peak in the $\phi\phi$ D-wave at 2300–2340 MeV. This makes a natural candidate for the $^3F_2$ $s\bar{s}$ partner of $f_2(2020)$.

Production of the $\phi\phi$ resonances from initial $\bar{p}p$ and $\pi\pi$ states requires explanation. It could arise if resonances are strongly mixed between $q\bar{q}$ and $s\bar{s}$. However, the small flavour mixing angles we observe do not point that way.

A second clear possibility is that the mixing is with the 2^+ glueball predicted in this mass range, or slightly above, by Lattice QCD calculations. There is evidence from the Crystal Barrel data on $\bar{p}p \to \eta\eta\pi^0$ for a broad 2^+ state in $\eta\eta$ with a mass of 1980 ± 50 MeV and a width $\Gamma = 500 \pm 100$ MeV [29]. There is similar evidence from two other sources. Firstly, a broad 2^+ contribution to the 4π channel is observed in central production data at small p_T [30]. Its mass is 1920 ± 20 MeV with a width of 450 ± 60 MeV. Secondly, there are data from BES on $J/\Psi \to \gamma 4\pi$ [41] and $J/\Psi \to \gamma K^* \bar{K}^*$ [42], which both require a broad 2^+ signal peaking at about 2000 MeV. The presence of this wide 2^+ signal in J/Ψ radiative decays and central production data is suggestive of mixing between a glueball and neighbouring $q\bar{q}$ states to produce a broad state.

We have tried inserting a broad $f_2(1980)$ with $\Gamma = 500$ MeV into our analysis, in addition to the four 2^+ states discussed above. There is a modest improvement in χ^2 of ~ 100, but little visible change to the quality of the fits. This is not sufficient to confirm the possible presence of a broad 2^+ background in the present data, because of the complexity of possible interferences with $f_2(1910)$ to $f_2(2300)$.

5.1 $f_0(2105)$

One very striking result of the present analysis is that $f_0(2105)$ is far from being a normal $q\bar{q}$ state. Its flavour mixing angle Φ is $+(59 - 64)^\circ$ if $f_0(2005)$ is excluded from the fit, or $+(68 - 71.6)^\circ$ with it included. That is, it behaves predominantly as an $s\bar{s}$ state. Allowing for interferences with $f_0(2005)$, it makes up $(4.6 \pm 1.5)\%$ of the $\pi^0\pi^0$ $J^P = 0^+$ intensity and $(38 \pm 5)\%$ of that for $\eta\eta$. The branching ratio to $\eta\eta'$ is not well determined, because of the low statistics in this channel. Our best estimate of amplitude ratios is as follows:

$$\pi^0\pi^0 : \eta\eta : \eta\eta' = 0.71 \pm 0.17 : 1 : -0.85 \pm 0.45. \tag{15}$$

For an unmixed $q\bar{q}$ state, the ratio expected between $\pi^0\pi^0$ and $\eta\eta$ is 0.8^{-4}, i.e. 2.44. The strong production of an $s\bar{s}$ state in $\bar{p}p$ annihilation is clearly anomalous. How can this be explained?

It could be a second glueball. A glueball would have a mixing angle of $+37^\circ$. The flavour mixing angle we observe then required some mixing with a nearby $s\bar{s}$ state; for ideal mixing, $s\bar{s}$ states are members of SU(3) singlets, so such mixing is plausible. The latest Lattice QCD calculations [43] predict a second 0^+ glueball with a mass ratio to the first of 1.54 ± 0.11. If we assign $f_0(1500)$ and $f_0(2105)$ as the two glueballs, the mass ratio is 1.40.

The alternative scenario, developed by Anisovich and Sarantsev [44], is that the glueball mixes strongly with neighbouring $q\bar{q}$ and $s\bar{s}$ states to generate a broad state which contains $\sim 50\%$ of the glueball in its wave function. Such a broad state may well overlap the mass range of the $f_0(2105)$. The $f_0(1500)$, $f_0(1770)$ and $f_0(2105)$ are all seen strongly as peaks in J/Ψ radiative decay to 4π [28]. This suggests that $f_0(2105)$ may be a mixed state made by mixing of the glueball with a nearby $s\bar{s}$ state. It is important to look for it in decays to $K\bar{K}$.

6 Conclusions

A combined analysis of the $\pi^-\pi^+$ data of Eisenhandler et al. and Hasan et al. with Crystal Barrel data for $\pi^0\pi^0$, $\eta\eta$ and $\eta\eta'$ leads to a secure partial wave analysis and the identification of

most of the expected $q\bar{q}$ resonances in this mass range, except for two 1^- states. The polarisation data play a vital role in separating states with $L = J \pm 1$. The resulting fit is rather close to that obtained previously by Hasan and Bugg [9]. However, it is now possible to identify clearly four 2^+ resonances. These have small flavour mixing and are probably to be identified with the $q\bar{q}$ $^3P_2$ and $^3F_2$ states expected in this mass range.

The systematics of resonances on Fig. 10 establishes a valuable guide to masses to be expected to $q\bar{q}$ states. This should help in identifying intruder states of exotic character.

The $f_0(2105)$ make a large contribution to the $\eta\eta$ and $\eta\eta'$ data. It is not to be identified with a simple $q\bar{q}$ state, because of its $+(59–71.6)^\circ$ flavour mixing angle. This requires it to have a large $s\bar{s}$ and/or exotic component.

7 Acknowledgement

We thank the Crystal Barrel Collaboration for allowing use of the data. We acknowledge financial support from the British Particle Physics and Astronomy Research Council (PPARC). We wish to thank Prof. V. V. Anisovich for helpful discussions. The St. Petersburg group wishes to acknowledge financial support from PPARC and INTAS grant RFBR 95-0267. We wish to thank Dr. D. Peaslee for helpful discussions on the data of Dulude et al, and also concerning Regge trajectories.

References

[1] A. Anisovich et al., *Data on $\bar{p}p \to \pi^0\pi^0$, $\eta\eta$ and $\eta\eta'$ from 600 to 1940 MeV/c*, accompanying paper.

[2] E. Eisenhandler et al., Nucl. Phys. B98 (1975) 109.

[3] A.A. Carter et al., Phys. Lett. B67 (1977) 117.

[4] A. Hasan et al., Nucl. Phys. B378 (1992) 3.

[5] A.A. Carter, Nucl. Phys. B141 (1978) 467.

[6] A.D. Martin and M.R. Pennington, Nucl. Phys. B169 (1980) 216.

[7] B.R. Martin and D. Morgan, Nucl. Phys. B176 (1980) 355.

[8] B.R. Martin and G.C. Oades, Nucl. Phys. A483 (1988) 669.

[9] A. Hasan and D.V. Bugg, Phys. Lett. B334 (1994) 215.

[10] B.R. Martin and G.C. Oades, Preprint IFA-SP-98-1, HEPPH-9802261.

[11] W.M. Kloet and F. Myrher, Phys. Rev. D53 (1996) 6120.

[12] A. Anisovich et al., Nucl. Phys. A 651 (1999) 253.

[13] Particle Data Group, Euro. Phys. Journ. 3 (1998) 1.

[14] S.U.Chung, Phys. Rev. D48 (1993) 1225.

[15] G.F. Chew and F.E. Low, Phys. Rev. 101 (1956) 1570.

[16] V.V. Anisovich, Phys. Lett. B364 (1995) 195.

[17] D.V. Bugg, A.V. Sarantsev and B.S. Zou, Nucl. Phys. B471 (1996) 59.

[18] V.V. Anisovich, Yu.D. Prokoshkin and A.V. Sarantsev, Phys. Lett. B389 (1996) 388.

[19] F. Binon et al., Lett. Nu. Cim. 39 (1984) 41.

[20] A. Anisovich et al., Phys. Lett. B452 (1999) 180

[21] R.S. Dulude et al., Phys. Lett. 79B (1978) 329, 335.

[22] D. Alde et al., Z. Phys. C66 (1995) 379.

[23] D. Ryabchikov, private communication.

[24] D. Ryabchikov, AIP Conf. Proc. 432 (1998) 603.

[25] D. Alde et al., Phys. Lett. B241 (1990) 600.

[26] S.I. Beladidze et al., Z. Phys. C54 (1992) 367.

[27] T.A. Armstrong et al., Phys. Lett. B307 (1993) 394.

[28] D.V. Bugg et al., Phys. Lett. B353 (1995) 378.

[29] A. Anisovich et al., Phys. Lett. B449 (1999) 145.

[30] D. Barberis et al., Phys. Lett. B413 (1997) 217.

[31] C. Hodd, Ph.D. Thesis, University of London (1999).

[32] J. Adomeit et al., Zeit. Phys. C71 (1996) 227.

[33] N. Isgur and J. Paton, Phys. Rev. D31 (1985) 2910.

[34] G. Höhler, F. Kaiser, R Koch and E. Pietarinen, *Handbook of Pion-Nucleon Scattering*, Univ. of Karlsruhe report TKP 78-11 (1978).

[35] A. Donnachie, Yu. S. Kalishnikova and A.B. Clegg, Zeit. Phys. C60 (1993) 187.

[36] D. Aston et al., Nucl. Phys. B21 (1991) 5 (suppl).

[37] A. Etkin et al., Phys. Lett. B201 (1988) 568.

[38] L. Bertolotto et al., Nucl. Phys. B (Proc. Suppl.) 56A (1997) 256.

[39] Yu. D. Prokoshkin, *Hadron 89*, Eds. F. Binon, J.-M. Frère and J.-P. Peigneux (Editions Frontières. Gif-sur-Yvette, France 1989) 27.

[40] D. Barberis et al., Phys. Lett. B453 (1999) 305.

[41] X. Shen, AIP Conf. Proc. 432 (1998) 47.

[42] L.Y. Dong, private communication.

[43] C.J. Morgenstern and M. Peardon, *The Glueball Spectrum from an isotropic lattice study*, hep-lat/99010004v2 and UCSD/PTH/98-36.

[44] V.V. Anisovich and A.V. Sarantsev, Phys. Lett. B382 (1996) 429.